Contents lists available at ScienceDirect

Physics of the Earth and Planetary Interiors

journal homepage: www.elsevier.com/locate/pepi

Amplitude and decay of long-period coda of great earthquakes

Han Xia (Hank)[a,b], Xiaodong Song[b,*], Richard Weaver[c], Jiangtao Li[b]

[a] Institute of Geophysics and Geodynamics, School of Earth Science and Engineering, Nanjing University, China
[b] Department of Geology, University of Illinois at Urbana-Champaign, USA
[c] Department of Physics, University of Illinois at Urbana-Champaign, USA

ABSTRACT

The earthquake coda is the residual vibration energy long after the main arrivals of an earthquake. Previous studies of coda waves have focused on high frequencies and small earthquakes, which are generally attributed to the scattering from the Earth's internal heterogeneities. Here we examined the early coda of great earthquakes at long periods (50 to 300 s) at time window of 10,000 to 50,000 s after the origin time. We used 10 major earthquakes (magnitude > 8.0) in recent decades that were recorded at global seismic networks. We found that the coda energy can be well represented by a simple exponential decay model for the early coda. The variation of the initial coda energy with distance is dominated by the effect of geometric spreading, suggesting that the scattering of the Earth's internal heterogeneities contributes little to the long-period early coda. The energy decay rate is largely insensitive to earthquake source (location, magnitude, focal mechanism, or rupture process), station location, or 3D variation of the earth's internal structure, making it ideal to constrain the average global attenuation structure. A small modification of the quality factor based on a global reference model can fit the coda energy decay well. The long-period coda energy may potentially provide a new way to determine the seismic moment of a major earthquake.

1. Introduction

The earthquake coda is the residual ground vibration energy that decays slowly after the main arrivals of an earthquake. It is generally thought to originate from the scattering of seismic waves as a result of material heterogeneities inside the earth. Different theories have been proposed to explain the generation of earthquake coda, including the single scattering theory applicable to the case of weak scattering (Aki, 1969) and the diffusion theory adequate for the case of strong scattering (Wesley, 1965). Both theories were based on the assumptions of isotropic scattering of scalar waves (no wave conversion), spherical source radiation and a homogeneous, isotropic and random distribution of scatters. A distinct feature of coda waves is their averaging effect on the source radiation pattern and local velocity heterogeneities, which results in a more stable energy envelope (Mayeda, 1993; Mayeda et al., 2003). Coda is composed of scattered waves that sample a volume containing both source and receiver and average the effects of geologic path variation, source-radiation pattern, and directivity. This averaging effect is similar to averaging direct waves over a well-distributed seismic network (Mayeda and Walter, 1996). As a result, using coda can achieve similar performance in estimating seismic moment and energy from a single station as when using network-averaged direct phases, which can reduce the influence of complicated 3-D heterogeneities.

A number of efforts have been made to understand the coda waves and the scattering process (e.g. Aki and Chouet, 1975; Rautian and Khalturin, 1978; Aki, 1981; Su et al., 1991). Furthermore, the decay of earthquake coda provides important information for the generation and propagation of coda waves and the earth's structure, especially the attenuation structure. Previous studies of coda have generally focused on high frequencies and small earthquakes by using the envelope of local earthquake coda to study earthquake magnitude or moment (Suteau and Whitcomb, 1979; Izutani and Kanamori, 2001; Mayeda and Walter, 1996; Baltay et al., 2010) and regional attenuation and scattering (Chouet, 1979, 1990; Korn, 1988, 1990, 1993, 1997; Wang and Shearer, 2017). Studies for long period coda have been quite limited. However, fundamental mode Rayleigh waves (up to R5) can be clearly observed and the envelope of Rayleigh waves and long period coda in a few hours after the earthquake has been modeled by single isotropic scattering model (Sato and Nohechi, 2001; Maeda et al., 2006) or multiple isotropic scattering model (Sato and Nishino, 2002). The later coda (after 20,000–35,000 s) can be modeled by higher-mode waves with smaller attenuation (Maeda et al., 2006; Poli et al., 2017).

Recent studies show that large earthquake coda at long periods contributes to the body waves extracted from ambient noise or earthquake coda cross-correlation (Lin and Tsai, 2013; Xia et al., 2016) and auto-correlation (Wang et al., 2015; Poli et al., 2017), especially for seismic phases from the earth's core. These studies suggest a large earthquake may generate a global long-period noise field in its coda that sample the deep interior of the Earth. In this study, we examine coda waves of great earthquakes at long periods (50 to 300 s), at a time

* Corresponding author.
E-mail address: xiao.d.song@gmail.com (X. Song).

https://doi.org/10.1016/j.pepi.2020.106538
Received 15 January 2020; Received in revised form 6 June 2020; Accepted 6 June 2020
Available online 09 June 2020

Table 1
List of large earthquakes used in this study.

Event	Date	Time (GMT)	Lat (°)	Lon (°)	Depth (km)	Mag (Mw)	Strike (°)	Dip (°)	Slip (°)	Event name (location)
1	2011/03/11	05:47:32	37.52	143.05	20.0	9.1	25	80	90	Tohoku, Japan
2	2004/12/26	00:58:52	3.41	95.90	28.6	9.0	129	83	87	Sumatra-Andaman Islands, Indonesia
3	2010/2/27	06:34:13	36.15	−72.93	28.1	8.8	172	74	82	Offshore Bio-Bio, Chile
4	2005/03/28	16:09:35	2.10	97.11	30.0	8.6	125	83	86	Northern Sumatra, Indonesia
5	2012/04/11	08:38:37	2.24	93.01	26.3	8.6	289	85	166	Offshore northern Sumatra
6	2001/06/23	20:33:09	16.30	−73.56	2.2	8.4	159	74	98	Near coast of southern Peru
7	2013/05/24	05:44:49	54.81	153.39	611.0	8.3	12	79	−89	Sea of Okhotsk
8	2015/09/16	22:54:32	31.53	−71.67	22.4	8.3	166	72	83	West of Illapel, Chile
9	2014/04/01	23:46:47	19.62	−70.79	17.1	8.1	159	76	86	Northwest of Iquique, Chile
10	2017/09/08	04:49:21	15.07	−93.72	69.7	8.1	318	78	−93	Southwest Of Tres Picos, Mexico

window long (10,000 to 50,000 s) after the earthquakes, to understand the generation and propagation of the coda waves. We found that the nature of the long-period coda waves is fundamentally different from that of the high-frequency coda waves from small earthquakes in previous studies. The coda energy is axisymmetric, indicating that the wave field is not fully diffused. The decay of the long-period coda energy is not sensitive to the 3D heterogeneity of the Earth and can be attributed mostly to the average attenuation structure of 1D earth.

2. Data and method

We selected 10 major earthquakes in different parts of the world from 2000 to 2017 with moment magnitude (Mw) > 8.0 (Table 1). We obtained the waveform data of these events recorded at 120 permanent stations of Global Seismic Network (GSN, with II and IU network codes) from Incorporated Research Institutions for Seismology (IRIS; Fig. 1). The GSN has a long deployment history, a global coverage and high-quality records, making it an excellent data set to study global coda waves of major earthquakes. We downloaded two days of continuous broadband data that contained the origin time of the event. We used three components of the seismograms for testing purpose and only the vertical component for the rest of the study.

We applied some basic data preprocessing that included removing instrument response, transforming to displacement record, and low-pass filtering with corner period of 10 s. We then calculated the power spectral density (PSD) of a moving time window using a time-frequency method (Cohen, 1995). Essentially, at time t of the coda wave with a moving step of 50 s, we chose a time window of 800 s centered at t, calculated the PSD of the time window at each (angular) frequency (the square of the spectral amplitude at the selected frequency), and obtained the average PSD over frequencies between 20% below and above (i.e. 0.8 to 1.2 times) the selected frequency. The averaging reduces the fluctuations of the PSD with frequency. We regard the average PSD as the energy ($E(t\,|\,\omega)$) of the coda wave at time t and (angular) frequency ω (Fig. 2).

Fig. 2 shows the typical behavior of the coda energy decay with time after a great earthquake. At about 10,000–20,000 s, although we can still observe fluctuations of wave packets, individual arrivals (seismic phases) cannot be identified and associated with. The logarithm of the energy decays nearly linearly with a similar rate to approximately 50,000. It continues to decay at the later time but more slowly. In this study, we used only the 10,000 to 50,000 s segment with nearly linear decay in the logarithm. The exponential decay of amplitude (energy) is expected from attenuation of a system with constant Q (Aki and Chouet, 1975; Weaver, 1987). We thus assume the following simple exponential decay model for the coda energy.

$$E(t \mid \omega) = E_0(\omega)e^{-\delta(\omega)t}. \quad (1)$$

In the logarithmic form (natural logarithm),

$$\ln[E(t \mid \omega)] = \ln[E_0(\omega)] - \delta(\omega)t. \quad (2)$$

where $E(t \mid \omega)$ is the coda energy (average PSD) for angular frequency ω at lapse time t, $E_0(\omega)$ is the extrapolated initial energy at the original time of the earthquake, $\delta(\omega)$ is earthquake coda energy decay coefficient. The decay coefficient dominates the trend of the coda energy decay and depends on frequency $\delta = \frac{\omega}{Q_c}$, where $1/Q_c$ describes earthquake coda attenuation and Q_c is the coda quality factor. From Eq. (2), we can obtain the decay coefficient $\delta(\omega)$ and the logarithm of the initial energy $E_0(\omega)$ for each frequency from the slope and the intercept of the linear regression.

We calculated synthetic seismograms using direct-solution method (DSM), which is efficient for a 1D earth model (Kawai et al., 2006). We simulated 500,000 s after earthquake by using simple 1D Preliminary Reference Earth Model (PREM, Dziewonski and Anderson, 1981) as reference model. To get the synthetic coda decay coefficient and initial energy, we process the synthetic seismograms following the above method for real events.

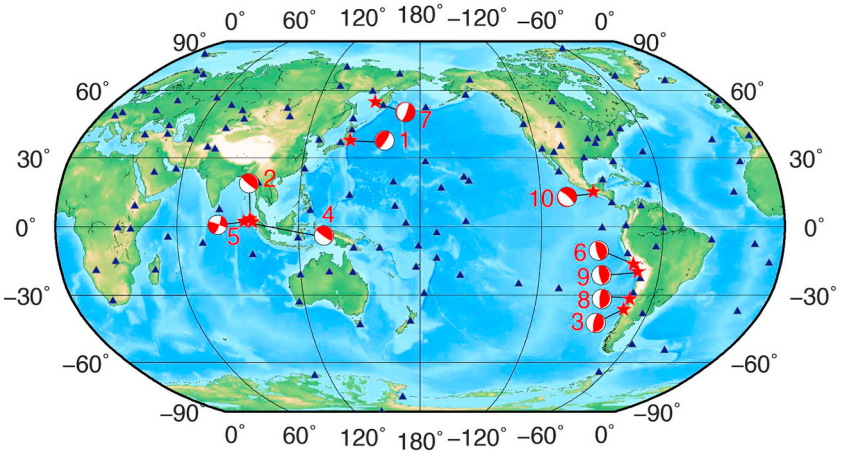

Fig. 1. Map of 10 great earthquakes (Mw ≥ 8.0, red stars) and 120 GSN stations (blue triangles) used in this study. The double-couple focal mechanism solutions of the great earthquakes (labeled) are also shown. (For interpretation of the references to color in this figure legend, the reader is referred to the web version of this article.)

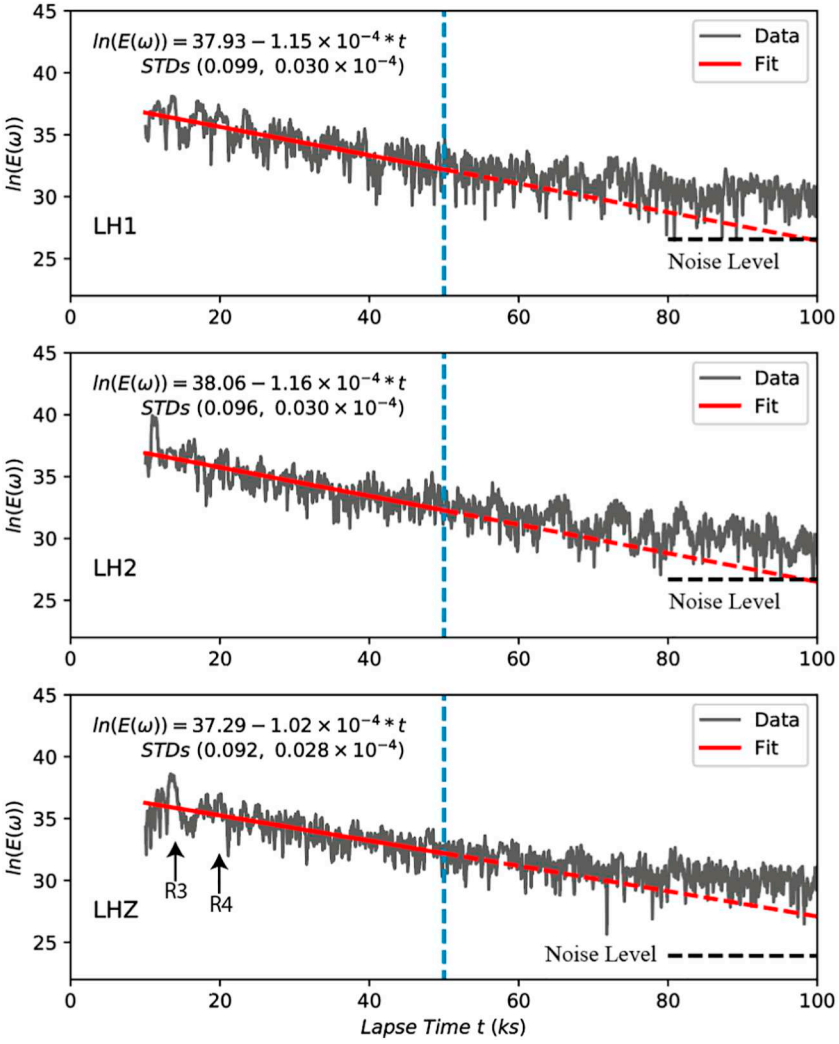

Fig. 2. Example of the coda energy of three components (two horizontal and one vertical from top to bottom panels) recorded by TAU station (at distance 80.15°) from event 1 (2011 Tohoku earthquake in Japan). The energy (for the period of 200 s) is in natural logarithm and the lapse time is relative to the origin time of the earthquake. The red line is linear regression (with the result and standard deviations of the coefficients noted) for the time window between 10,000 and 50,000 s (blue dashed vertical line). The linear regression is extrapolated (dashed line) to show better the slower decay rate of the later coda. Noise level from segments before the earthquake is indicated by the grey dashed line. Black arrows indicate arrival times of global Rayleigh phases R3 and R4. (For interpretation of the references to color in this figure legend, the reader is referred to the web version of this article.)

3. Results

3.1. Coda energy and decay rate

The example in Fig. 2 is fairly typical of all stations and all events. The coda energy data at lapse time 10,000 to 50,000 s can be well fitted by linear regressions. The results for three components of ground motions (vertical Z, north-south N, east-west E) are quite similar in the slope and the intercept of the linear regression. However, there are still some differences in the values that are much greater than the error estimates, which may be caused by the earthquake radiation pattern (see discussion below). In this study, we focused only the Z-component data. Compared with the N and E components, the Z component generally has better data quality (higher signal to noise ratio).

The decay coefficients are quite stable for different stations and different events (Fig. 3a). To remove a few poor quality records, we ignored the measurements that are outside two standard deviations from the mean decay coefficient of the event. The average from all the measurements of the decay coefficients of all the events is $(1.02 \pm 0.15) \times 10^{-4}$ (one standard deviation) at the period of 200 s. The average from each event is all within one standard deviation of the total average.

The initial energy term $\ln(E_0(\omega))$ shows clear distance-dependence "smiley" pattern with larger values at stations of smaller epicentral distances or near the antipode to the earthquake and smaller values at stations close to the distance of 90° (Fig. 3b). The axis-symmetric "smiley" pattern is indicative of the geometrical spreading of an energy flux (E_f) across the surface of the Earth, according to the following relationship:

$$E_f(\Delta) = E_f(0)/\sin(\Delta). \quad (3)$$

We thus introduce the corrected initial energy $E_0(\omega)$ for each station as

$$E_{0c}(\omega) = E_0(\omega) * \sin(\Delta). \quad (4)$$

or in logarithmic form:

$$\ln[E_{0c}(\omega)] = \ln[E_0(\omega)] + \ln[\sin(\Delta)]. \quad (5)$$

After removing the effect of geometric spreading, the corrected initial energy values $E_{0c}(\omega)$ from all stations are nearly the same for the same event (Fig. 3c). The levels for different events are offset by constant values, which are related to the magnitudes of the events. The results demonstrate that the variation of the initial energy with distance is dominated by the effect of simple geometrical spreading across the Earth's surface.

Fig. 4 summarizes the results on coda attenuation and energy for the 10 events in this study (for the period of 200 s). The attenuation values ($1/Q_c$) are quite similar for the all events (Mw from 8.1 to 9.1) at $(3.25 \pm 0.48) \times 10^{-3}$ (around an average Q_c of 313). The logarithm of corrected initial energy (E_{0c}) increases roughly linearly with the earthquake moment (Fig. 4b). It indicates that the initial energy is largely determined by the magnitude of an earthquake. All the events in

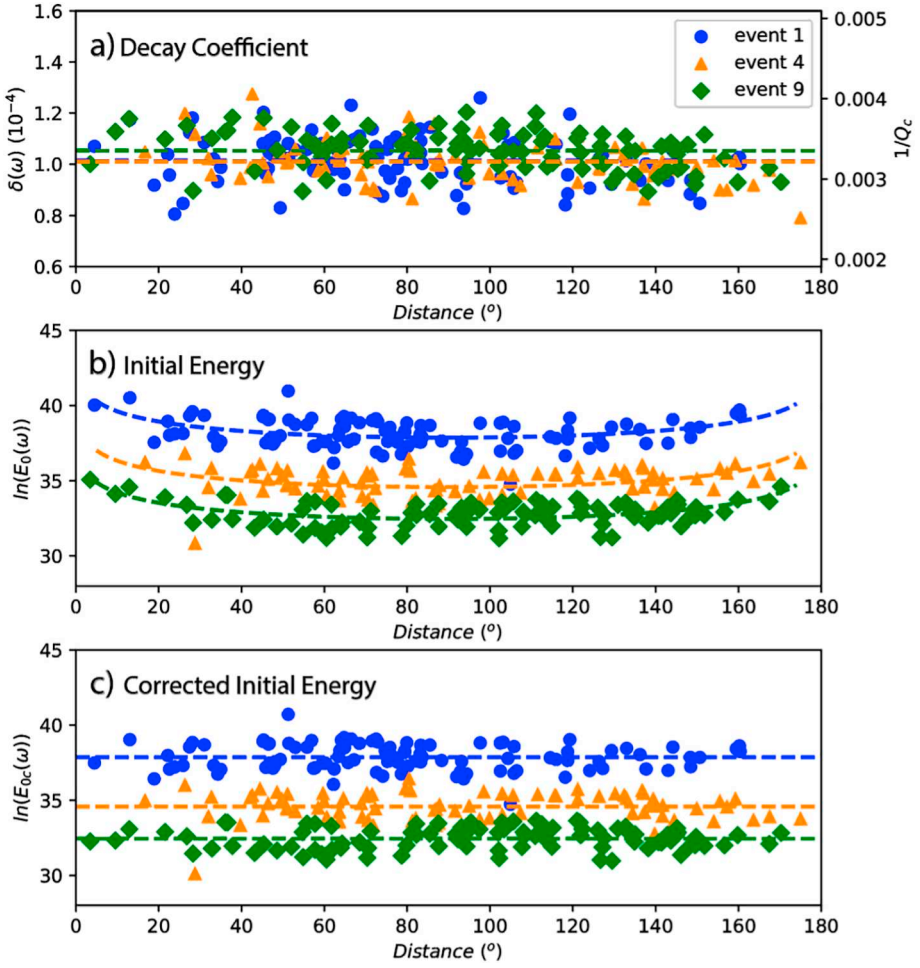

Fig. 3. Parameters from the simple exponential decay model of the coda energy (at period of 200 s) as a function of epicentral distance for three representative events (1, 4, and 9) of different magnitudes (Table 1). a) Coda energy decay coefficient and earthquake coda attenuation (left and right axes, respectively). The dashed line shows the average coda decay coefficient for each event. b) Initial coda energy (in logarithm). The dashed line is the prediction from the geometric spreading for each event (Eq. (5)). c) Corrected initial coda energy after removing the geometric spreading (Eq. (5)). The dashed line indicates the average value for each event.

this study are reverse faults except one strike-slip event (Table 1). The result for the strike-slip event (Fig. 4b, open triangle) seems somewhat different with those of other events. All the events are relatively shallow (< 70 km) except one event at depth of 611 km (event 7), which shows a slightly smaller $1/Q_c$ value (Fig. 4a).

3.2. Potential biases in estimating coda energy and decay rate

We examined factors that could bias the estimates of the coda energy and decay rate in the above, including focal mechanism, focal depth, and aftershock activity. Fig. 5 compares the azimuthal dependence of the corrected initial coda energy between the real data and the synthetics simulated by 1D PREM using the real focal mechanism from Global Centroid Moment Tensor Catalog (GCMT). The pattern from real earthquake (black points, Fig. 5) is consistent with that of the synthetic coda energy (grey points, Fig. 5). The results indicates that the initial coda energy in long period is dominated by energy along great circle rather than influence of the scattering structure, and complicated 3D earth's structure (e.g. heterogeneity, anisotropy and scatter structure) doesn't have significant effect to the initial energy. In the meanwhile, the azimuthal pattern caused by the earthquake moment tensor may explain the error bar and misfit in Fig. 4b. The azimuthal dependence pattern may be a new way to constrain the focal mechanism of a major earthquake, which can ignore the influence of complicate 3D structure.

The top three largest aftershocks among all the events within our coda time window are Mw 8.2, 7447 s after event 5 (Mw 8.6); Mw 7.9, 1706 s after event 1 (Mw 9.1); and Mw 7.4, 5175 s after event 3 (Mw 8.8), respectively. The rest of the aftershocks are less than Mw 7.1. The three highest ratios between the seismic moments of the largest aftershock and the main shock are 31.6% (event 5), 2.1% (event 9), and 1.6% (event 1). These aftershocks all occurred within 10,000 s after the main shock. Thus, using the empirical relationships for $\ln(E_{0c})$ and coda decay rate with respect to $\ln(M_0)$ (Fig. 4), we estimated the influence (contribution to the logarithm of energy) of about 1.03%, 0.01%, and 0.01% respectively, for events 5, 1 and 9 at the beginning of our coda window (10,000 s after the main shock).

We examined event 5 more closely because of its large aftershock (above) and possible influence of the strike-slip mechanism (Fig. 5c). The azimuthal pattern for the real data is similar to that for synthetic coda energy, but the simulated data show sharper azimuthal variation than the real data. The result indicates that the misfit for magnitude of event 5 (open triangle, Fig. 4b) may be affected by the strike-slip focal mechanism. To examine the influence of the large aftershock, we simulated the coda energy decay with and without the aftershock (Fig. S2) using the same source parameters as the real data. The coda energy and decay show some minor differences – the energy $\ln(E_{0c})$ without the aftershock is smaller by 0.81 and the slope is smaller by 10%. If we use these numbers to correct for event 5, the results agree better with the overall trends (Fig. 4). In particular, the $1/Q_c$ value agrees with the average very well (Fig. 4a), thus discrepancy of the initial coda attenuation measurement may not be influenced by the strike-slip mechanism. Because of relatively much smaller aftershocks for other

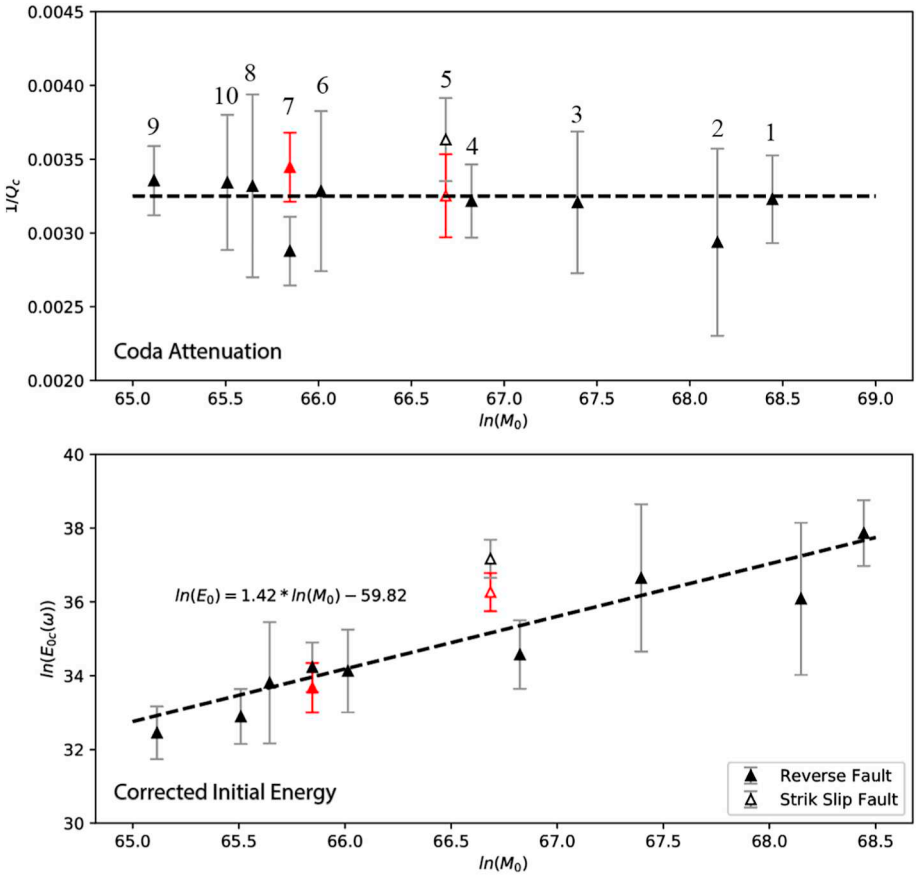

Fig. 4. Summary plot of coda attenuation (a) and corrected initial energy (b) for the 10 events (labeled) at 200 s. The black triangles and error bars show the mean value and one standard for every event. Two types of the focal mechanisms (reverse and strike-slip faults) of the 10 events are distinguished. The dashed lines in (a) and (b) are the average and the linear regression of all the events, respectively. The red triangles and error bars are results after correcting for the influence of a large aftershock for event 5 and source depth for the deep event 7 (see text). (For interpretation of the references to color in this figure legend, the reader is referred to the web version of this article.)

events, the influence is negligible (much smaller than the measurement errors).

We also examined the depth effect for the only deep event (event 7). We generated synthetics using 1D PREM model and DSM method for the same focal mechanism and depth and station distribution and measured $\ln(E_{0c})$ and $1/Q_c$ values as the real data. We repeated the process by keeping all the parameters the same except using a hypothetical shallow focus (depth of 20 km). The $\ln(E_{0c})$ value is smaller

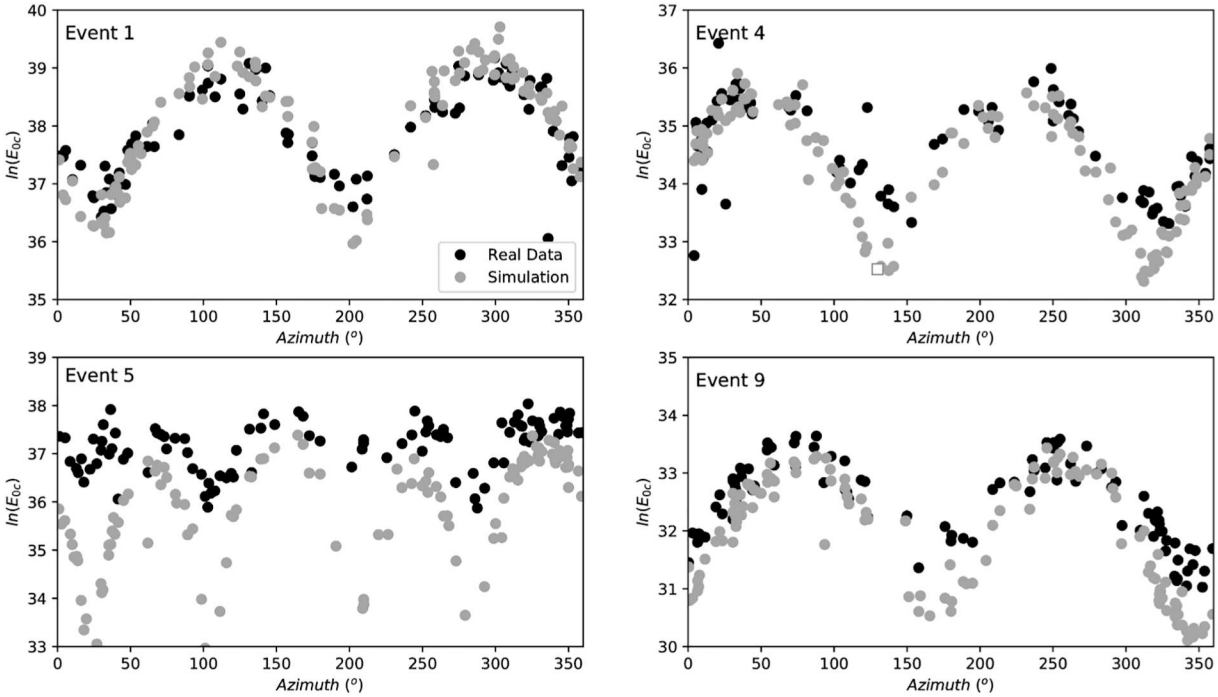

Fig. 5. Comparison of corrected initial coda energy (after removing the geometric spreading) as a function of azimuth (from epicentral to station) between real events (black) and synthetics (grey). Synthetic seismograms were calculated using DSM and 1D PREM.

by 0.56 and the $1/Q_c$ value is greater by 0.00057. Correcting for the difference improves the fit for the attenuation but the fit for the energy changes little (Fig. 4).

3.3. Generation of long-period coda wave

The results above show that the long-period coda wave (at 10,000–50,000 s) is axisymmetric. The Earth behaves as a one-dimensional isotropic medium for the coda energy, in which heterogeneity and anisotropy have been mostly averaged out. However, the coda wave is not fully diffuse because the coda energy (E_0) still contains the geometrical spreading effect. For a fully diffuse field, the energy is distributed uniformly and all points on the globe become equivalent such that the energy near the epicenter (or the antipode) is no longer enhanced over other distances (Weaver et al., 2017). The result suggests that, for the long periods and the relatively early coda, the scattering from the Earth's internal heterogeneity is too weak to produce a fully diffuse field. In fact, a 1D Earth without any heterogeneity or anisotropy can match the decay and the geometrical spreading effect of the coda energy (Fig. S1 and below). The non-diffuse characteristic of the long period coda of large earthquakes is consistent with previous studies (Sens-Schönfelder et al., 2015; Poli et al., 2017). Sens-Schönfelder et al. (2015) found that at periods of 10 to 40 s the late coda (of the Sea of Okhotsk deep earthquake, our event 7) is dominated by waves propagating along the great circle and that at over 40-s periods the coda envelopes are well explained by reverberations in a 1D-layered earth (PREM). Poli et al. (2017) also confirmed the predominance of great circle propagation in the late coda at intermediate periods (28–66 s).

The above results suggest the decay rate is not sensitive to station location or the 3D variation of the earth's internal structure. Neither it is sensitive to the geographical location, magnitude, focal mechanism, or rupture process of the earthquake, although it has minor sensitivity to earthquake depth. Thus, the decay rate can be used to infer the attenuation structure of the Earth (below). Furthermore, the coda energy potentially provides a new powerful way to determine the magnitude of a major earthquake, because (1) the corrected energy is not affected by 3D heterogeneity of the earth, (2) the corrected energy is stable among different stations, and (3) potentially only a single component of a single station is needed.

3.4. Global attenuation structure

Fig. 6 summarizes coda attenuation ($1/Q_c$) measurements from 8 events for periods from 50 s to 300 s (frequency from 3.3 to 20 mHz). We excluded events 5 and 7 for possible influence of aftershock and source depth (see above). However, if we include all the 10 events, the result is identical. The coda attenuation decreases from 0.0034 to 0.0060 (or Q_c increases from 300 to 1650) as frequency increases from 5 to 20 mHz, which generally agrees with the predictions simulated by DSM for 1D PREM model (Fig. 6). However, at lower frequencies, the PREM model over predicts the coda attenuation. If we adjust the global average Q model, we can improve the fit to the coda attenuation measurements. For example, we tested a simple model that is based on PREM but includes a 20% decrease of Q_μ in the asthenosphere layer in PREM (depth of 80–220 km) and 15% increase of Q_μ in the rest of the mantle. The predictions on the coda attenuation can generally fit the real observations, although further refinement can be made in the future. Note the azimuthal distribution of our global stations is quite uniform, thus our result is unlikely biased by sampling of the uncorrected focal mechanism effect.

Our result on the coda Q_c is somewhat different from previous studies by Maeda et al. (2006) and Sens-Schönfelder et al. (2015), both suggesting agreements with the PREM predictions. However, we used much more data with more great earthquakes, thus perhaps representing better the global average. Our analyses are more quantitative with detailed measurements and modeling. Furthermore, our parameters are somewhat different. Maeda et al. (2006) refers to the later coda (about 3500 to 7000) at 90–180 s and Sens-Schönfelder et al. (2015) refers to the coda from 0 to 35,000 s at periods over 32 s. Nevertheless, our modified Q model needs to be further tested and refined in the future, taking into more careful account of other factors (e.g., focal mechanism and depth, 3D structure, and surface topography).

3.5. Sensitivity for different depth's attenuation structure

To understand the sensitivity of coda attenuation for different depth's Q structure, we simulated the seismograms by the DSM with explosion source. We calculated the coda attenuation using a modified 1D model with value of Q_μ 10% increase for the layer of 50 km above and below the given depth compared with the reference model (PREM). The calculation was done for epicentral distances from 0.5° to 179.5° at 0.5°interval. We defined the sensitivity coefficient following the equation below:

$$S(\omega) = \left(\frac{1}{n} * \sum_{i=1}^{n} |Q_{mod}(i) - Q_{ref}(i)|\right) / \left(\frac{1}{n} * \sum_{i=1}^{n} |Q_{ref}(i)|\right). \quad (6)$$

where n is the total number of stations, $Q_{ref}(i)$ and $Q_{mod}(i)$ are the coda quality factor (Q_c) for reference model and the modified model, respectively.

Fig. 7 shows that the sensitivity coefficient is almost zero on the depth > 800 km for different frequency, which indicated the long-period coda attenuation in this study is dominated by the quality factor

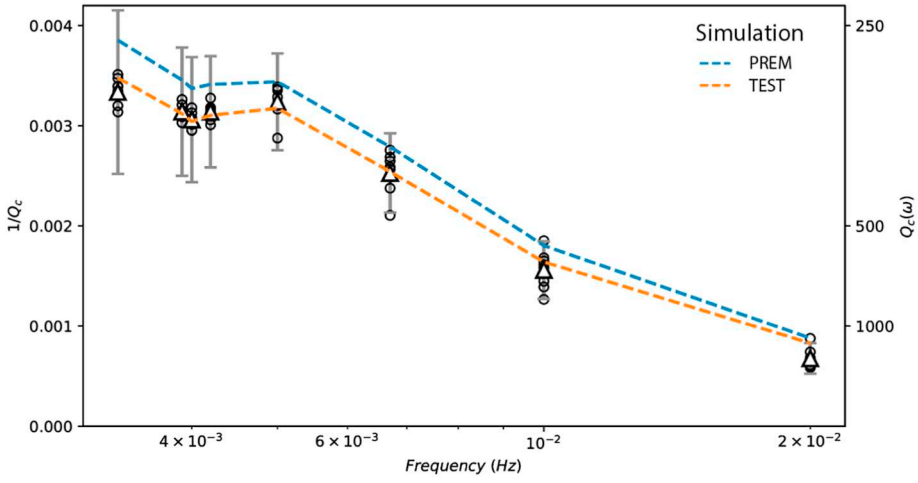

Fig. 6. Coda attenuation as a function of frequency. The circle shows the average of coda attenuation for each individual event. We excluded event 5 (strike-slip) and event 7 (deep event). The triangle and error bar show the mean and ± one standard deviation of the measurements from all the 8 events and stations for the corresponding frequency. The dashed lines are predictions for the PREM (blue) and a test model (TEST, orange). The TEST model was based on the PREM with 20% reduction in Q value in the asthenosphere (depth of 80–220 km) and 15% increase in the rest of the mantle. Note the standard deviation of the mean for each frequency is very small with the largest one being 0.00006 (for 300 s), which is hardly visible if plotted. (For interpretation of the references to color in this figure legend, the reader is referred to the web version of this article.)

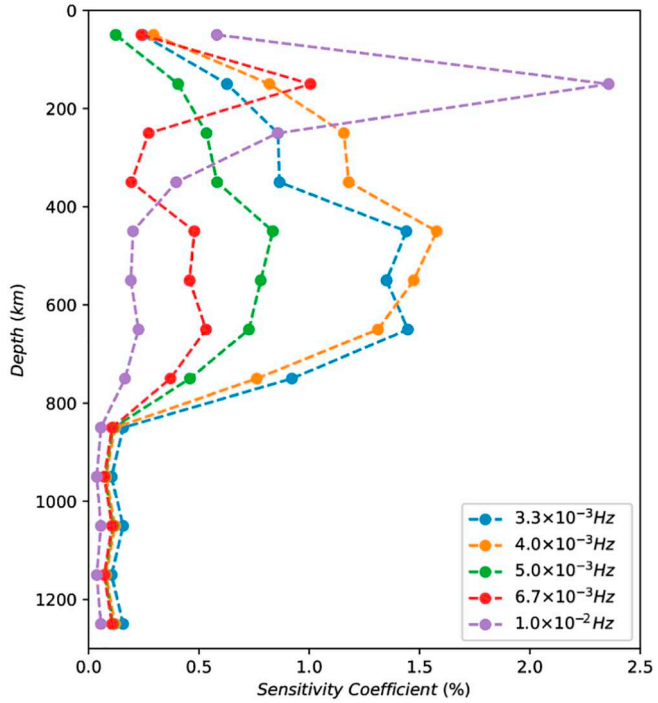

Fig. 7. The sensitivity of coda energy decay coefficient to the attenuation structure at different depths. The color solid circles show the sensitivity coefficients of coda quality factor for different frequencies (labeled). The sensitivity coefficient is calculated according to Eq. (6). (For interpretation of the references to color in this figure legend, the reader is referred to the web version of this article.)

above upper mantle, and hardly sample the attenuation structure of lower mantle and core of the earth. For higher frequency (6.7 mHz, 10.0 mHz), sensitivity coefficient is > 1% for shallow attenuation (100–200 km), and smaller than 0.5% for deep attenuation (400–700 km). The sensitivity coefficient of coda quality factor on lower frequency (3.3 mHz, 4.0 mHz) is around 1.5% for deep attenuation (400–700 km). It indicates that the longer period coda quality factor is more sensitive to the attenuation at greater depth and the higher frequency coda decay ratio is dominated by the shallow attenuation structure. Thus, the coda quality factors at different frequencies in the future will help constrain the fine structure of the global average attenuation, especially at the upper mantle.

3.6. Accuracy of long-period coda from DSM synthetics

The DSM method (Kawai et al., 2006) provides an efficient method to calculate our long-period coda waves for 1D models. Such efficiency is particularly important where a large amount of computation is required (such as modeling). The DSM method has been widely used, but we are not aware of its usage for long-period coda of great earthquakes, which vary greatly (orders of magnitude) in amplitudes (i.e., a wide dynamic range). To examine the accuracy of the DSM for long period coda, we compared the simulated coda energy from the DSM and the spectral element method for 3D earth (SPECFEM3D_GLOBE) (Komatitsch and Tromp, 2002). We used the same source and station distribution as event 1 (Table 1) for the simulations. We used 1D reference model PREM for both methods and exclude ocean, topography, gravity and rotation in SPECFEM3D so that the model for both methods are the same. The simulated coda from the two methods are highly similar (Fig. S3a). The retrieved coda energy and attenuation show some difference in individual measurements (Fig. S3b), but the mean is negligible, compared to the scatter of the real observations. The mean and standard deviation are −0.14 and 0.12 for initial coda energy (ln(E_0)), respectively, and 0.97 × 10^{-4} and 1.45 × 10^{-4} for coda attenuation ($1/Q_c$), respectively. Thus, the mean difference is 0.4% and 2.8% in initial coda energy (ln(E_0)) and coda attenuation ($1/Q_c$), respectively. We conclude that the DSM method is sufficiently accurate for the long-period coda analyses.

4. Conclusion and discussion

We examined long-period (50 to 300 s) coda waves of 10 great earthquakes (2000 to 2017, Mw > 8.0). The coda energy decay at time window 10,000 to 50,000 s for long periods (50 to 300 s) can be explained by a simple exponential decay model. We found that the generation of the long-period coda does not require scattering as proposed previously (Sato and Nohechi, 2001; Sato and Nishino, 2002; Maeda et al., 2006). The logarithm of the initial coda energy ln(E_0) shows a clear distance-dependent "smiley" pattern that is dominated by the simple geometric spreading, suggesting that the scattering of the Earth's internal heterogeneity (which would homogenize the wave field and make it diffuse) contributes little to the long-period coda. The coda energy comes mainly from the reverberations and conversions from the Earth's internal discontinuities. While the scattering model does not really fit the envelope or the decay of the long-period early coda (Sato and Nohechi, 2001; Sato and Nishino, 2002; Maeda et al., 2006), synthetics from a simple 1D earth model (without any lateral heterogeneity) can fit the coda envelope and decay well. The non-diffuse nature of the long-period coda of great earthquakes needs to be considered in the coda wave interferometry (Sens-Schönfelder et al., 2015; Poli et al., 2017).

The energy decay coefficient $\delta(\omega)$ is largely insensitive to earthquake source (location, magnitude, focal mechanism, or rupture process), station locations, or 3D variation of the earth's internal structure. It is dominated by the average global attenuation structure. In fact, an isotropic 1D Earth can match the decay and the geometrical spreading effect of the coda energy. A simple modification of the global average Q model based on PREM (Fig. 5) can match the coda decay well. The coda energy decay coefficient is more sensitive to the Q structure in upper mantle for the frequencies used in this study. The higher frequency coda decay coefficient provides more constraint for the shallower depth Q structure. As a consequence, further improvement can be made to constrain the global average Q structure, especially the Q structure in the upper mantle. Consequently, the long-period coda attenuation provides an excellent way to constrain the global average Q model that is independent of earthquakes, stations, and complicated 3D structure.

The logarithm of the corrected initial energy (E_{0c}) is almost linearly correlated with the logarithm of the earthquake moment. Consequently, using the corrected initial energy from the earthquake coda may provide a new way to determine the magnitude and moment tensor of a major earthquake. Such a measure can avoid or limit the influences of station distribution and the 3D heterogeneity of the Earth.

In developing such a measure, the following factors are likely important, which need to be properly taken into account. (1) Focal mechanism. Simple synthetic tests using the DSM (Kawai et al., 2006) and a 1D isotropic Earth model suggest a clear azimuthal variation of the coda energy (at the same distance), which varies with focal mechanism. The azimuthal pattern of corrected initial energy can be a new way to constrain the focal mechanism of the major earthquake. Focal mechanism also affects the relative amplitudes of the coda energy between different components of the ground motion. For example, an explosion source would not generate any energy in the tangential component for an isotropic 1D Earth as expected. (2) Frequency dependence of the coda energy. The coda attenuation is relatively stable with respect to frequency (Fig. 6). Thus, the coda energy for different frequency can be combined to determine the magnitude of the event. (3) Time window for the coda energy. We chose a time window (10,000–50,000 s) in which the logarithm of the coda energy decays nearly linearly. Other models can be found to fit the coda energy in a longer time window,

which would improve the understanding of the coda decay and the measurement accuracy of the coda energy.

CRediT authorship contribution statement

Han Xia: Methodology, Formal analysis, Writing - original draft.**Xiaodong Song:**Conceptualization, Formal analysis, Resources, Writing - review & editing, Supervision.**Richard Weaver:**Conceptualization, Validation, Formal analysis.**Jiangtao Li:**Validation, Formal analysis.

Declaration of competing interest

We declare that no support, financial or otherwise, has been received from any organization that have an interest in the submitted work, and there are no other relationships or activities that could appear to have influence the submitted work.

Acknowledgments

The waveform data were obtained from the IRIS DMC. We thank two anonymous reviewers and the Editor for insightful reviews, which improves the manuscript greatly. This research was supported by the National Natural Science Foundation of China (U1939204) and the National Science Foundation of the United States (EAR 1620595).

Appendix A. Supplementary data

Supplementary data to this article can be found online at https://doi.org/10.1016/j.pepi.2020.106538.

References

Aki, K., 1969. Analysis of the seismic coda of local earthquakes as scattered waves. J. Geophys. Res. 74, 615–631.
Aki, K., 1981. Source and scattering effects on the spectra of small local earthquakes. Bull. Seismol. Soc. Am. 71, 1687–1700.
Aki, K., Chouet, B., 1975. Origin of coda waves: source, attenuation, and scattering effects. J. Geophys. Res. 80, 3322–3342.
Baltay, A., Prieto, G., Beroza, G.C., 2010. Radiated seismic energy from coda measurements and no scaling in apparent stress with seismic moment. J. Geophys. Res. 115, B08314.
Chouet, B., 1979. Temporal variation in the attenuation of earthquake coda near Stone Canyon, California. Geophys. Res. Lett. 6, 143–146.
Chouet, B., 1990. Effect of anelastic and scattering structures of the lithosphere on the shape of local earthquake coda. Pure Appl. Geophys. 132, 289–310.
Cohen, L., 1995. Time-frequency Analysis. Prentice Hall, pp. 778.
Dziewonski, A.M., Anderson, D.L., 1981. Preliminary reference Earth model. Phys. Earth Planet. Inter. 25, 297–356.
Izutani, Y., Kanamori, H., 2001. Scale-dependence of seismic energy-to-moment ratio for strike-slip earthquakes in Japan. Geophys. Res. Lett. 28, 4007–4010.
Kawai, K., Takeuchi, N., Geller, R.J., 2006. Complete synthetic seismograms up to 2 Hz for transversely isotropic spherically symmetric media. Geophys. J. Int. 164, 411–424.
Komatitsch, D., Tromp, J., 2002. Spectral-element simulations of global seismic wave propagation - I. Validation. Geophys. J. Int. 149, 390–412.
Korn, M., 1988. P-wave coda analysis of short-period array data and the scattering and absorptive properties of the lithosphere. Geophys. J. 93, 437–449.
Korn, M., 1990. A modified energy flux model for lithospheric scattering of teleseismic body waves. Geophys. J. Int. 102, 165–175.
Korn, M., 1993. Determination of site-dependent scattering Q from P -wave coda analysis with an energy-flux model. Geophys. J. Int. 113, 54–72.
Korn, M., 1997. Modelling the teleseismic P coda envelope: depth dependent scattering and deterministic structure. Phys. Earth Planet. Inter. 104, 23–36.
Lin, F.C., Tsai, V.C., 2013. Seismic interferometry with antipodal station pairs. Geophys. Res. Lett. 40, 4609–4613.
Maeda, T., Sato, H., Ohtake, M., 2006. Constituents of vertical-component coda waves at long periods. Pure Appl. Geophys. 163, 549–566.
Mayeda, K., 1993. A stable single station estimator of magnitude. Bull. Seismol. Soc. Am. 83, 851–861.
Mayeda, K., Walter, W.R., 1996. Moment, energy, stress drop, and source spectra of western United States earthquakes from regional coda envelopes. J. Geophys. Res. Solid Earth 101, 11195–11208.
Mayeda, K., Hofstetter, A., O'Boyle, J.L., Walter, W.R., 2003. Stable and transportable regional magnitudes based on coda-derived moment-rate spectra. Bull. Seismol. Soc. Am. 93, 224–239.
Poli, P., Campillo, M., de Hoop, M., 2017. Analysis of intermediate period correlations of coda from deep earthquakes. Earth Planet. Sci. Lett. 477, 147–155.
Rautian, T.G., Khalturin, V.I., 1978. The use of the coda for determination of earthquake source spectrum. Bull. Seismol. Soc. Am. 64, 923–948.
Sato, H., Nishino, M., 2002. Multiple isotropic-scattering model on the spherical Earth for the synthesis of Rayleigh-wave envelopes. J. Geophys. Res. Solid Earth 107 ESE 7.
Sato, H., Nohechi, M., 2001. Envelope formation of long-period Rayleigh waves in vertical component seismograms: single isotropic scattering model. J. Geophys. Res. Solid Earth 106, 6589–6594.
Sens-Schönfelder, C., Snieder, R., Stähler, S.C., 2015. The lack of equipartitioning in global body wave coda. Geophys. Res. Lett. 42, 7483–7489.
Su, F., Aki, K., Biswas, N.N., 1991. Discriminating quarry blasts from earthquakes using coda waves. Bull. Seismol. Soc. Am. 81, 162–178.
Suteau, A.M., Whitcomb, J.H., 1979. A Local Earthquake Coda Magnitude and its Relation to Duration, Moment M0, and Local Richter Magnitude ML 69, 353–368.
Wang, W., Shearer, P.M., 2017. Using direct and coda wave envelopes to resolve the scattering and intrinsic attenuation structure of Southern California. J. Geophys. Res. Solid Earth 122, 7236–7251.
Wang, T., Song, X., Xia, H.H., 2015. Equatorial anisotropy in the inner part of Earth's inner core from autocorrelation of earthquake coda. Nat. Geosci. 9512, 1–4.
Weaver, R.L., 1987. Indications of Material Character from the Behavior of Diffuse Ultrasonic Fields. In: Bussière, J.F., Monchalin, JP., Ruud, C.O., Green, R.E. (Eds.), Nondestructive Characterization of Materials II. Springer, Boston, MA, pp. 689–695.
Weaver, R.L., Yoritomo, J.Y., Coleman, J.P., 2017. Diffuse elastic waves in a nearly axisymmetric body: energy distribution, transport and dynamical localization. Eur. Phys. J. Spec. Top. 226, 1371–1408.
Wesley, J.P., 1965. Diffusion of seismic energy in the near range. J. Geophys. Res. 70, 5099–5106.
Xia, H.H., Song, X., Wang, T., 2016. Extraction of triplicated PKP phases from noise correlations. Geophys. J. Int. 205, 499–508.